

# Cold Ageing of NMC811 Lithium-ion Batteries

Wang, C., Amietszajew, T., Carvajal, R., Guo, Y., Ahmed, Z., Zhang, C., Goodlet, G. & Bhagat, R.

Published PDF deposited in Coventry University's Repository

**Original citation:**

Wang, C, Amietszajew, T, Carvajal, R, Guo, Y, Ahmed, Z, Zhang, C, Goodlet, G & Bhagat, R 2021, 'Cold Ageing of NMC811 Lithium-ion Batteries', *Energies*, vol. 14, no. 16, 4724.

<https://dx.doi.org/10.3390/en14164724>

DOI 10.3390/en14164724

ESSN 1996-1073

Publisher: MDPI

**This is an open access article distributed under the Creative Commons Attribution License which permits unrestricted use, distribution, and reproduction in any medium, provided the original work is properly cited.**

## Article

# Cold Ageing of NMC811 Lithium-ion Batteries

Chongming Wang <sup>1,\*</sup>, Tazdin Amietszajew <sup>1</sup> , Ruth Carvajal <sup>1</sup>, Yue Guo <sup>1</sup>, Zahoor Ahmed <sup>1</sup>, Cheng Zhang <sup>1</sup>, Gregory Goodlet <sup>2</sup> and Rohit Bhagat <sup>1</sup>

<sup>1</sup> Institute for Future Transport and Cities, Coventry University, Coventry CV1 5FB, UK; taz.amietszajew@coventry.ac.uk (T.A.); ruthycus@gmail.com (R.C.); yue.guo@coventry.ac.uk (Y.G.); zahoor.ahmed@coventry.ac.uk (Z.A.); cheng.zhang@coventry.ac.uk (C.Z.); rohit.bhagat@coventry.ac.uk (R.B.)

<sup>2</sup> Johnson Matthey, Reading RG4 9NH, UK; gregory.goodlet@matthey.com

\* Correspondence: chongming.wang@coventry.ac.uk

**Abstract:** In the application of electric vehicles,  $\text{LiNi}_{0.8}\text{Mn}_{0.1}\text{Co}_{0.1}\text{O}_2$  (NMC811)—a Ni-rich cathode has the potential of replacing  $\text{LiNiMnCoO}_2$  (NMC111) due to its high energy density. However, NMC811 features relatively poor structural and thermal stabilities, which affect its cycle life. This study aims to address the limited data availability research gap on NMC811 low-temperature degradation. We aged commercial 21700 NMC811 cells at 0 °C under 0.5 C and 1 C current rates. After 200 cycles, post-mortem visual, scanning electron microscopy (SEM) and energy-dispersive X-ray (EDX) spectroscopy, the inspections of harvested electrodes were conducted. In just 200 cold cycles, capacity drops of 25% and 49% were observed in cells aged at 1 C and 0.5 C, respectively. The fast degradation at low temperatures is largely due to lithium plating at the anode side during the charging process. The surprisingly better performance at 1 C is related to enhanced cell self-heating. After subsequent 3-month storage, the cells that experienced 200 cycles at 0 °C and 0.5 C became faulty (voltage:  $\approx 0$  V), possibly due to cell lithium dendrites and micro short circuits. This work demonstrates that NMC811 suffers from poor cold ageing performance and subsequent premature end-of-life.



**Citation:** Wang, C.; Amietszajew, T.; Carvajal, R.; Guo, Y.; Ahmed, Z.; Zhang, C.; Goodlet, G.; Bhagat, R. Cold Ageing of NMC811 Lithium-ion Batteries. *Energies* **2021**, *14*, 4724. <https://doi.org/10.3390/en14164724>

Academic Editor: Alvaro Caballero

Received: 9 July 2021  
Accepted: 30 July 2021  
Published: 4 August 2021

**Publisher's Note:** MDPI stays neutral with regard to jurisdictional claims in published maps and institutional affiliations.



**Copyright:** © 2021 by the authors. Licensee MDPI, Basel, Switzerland. This article is an open access article distributed under the terms and conditions of the Creative Commons Attribution (CC BY) license (<https://creativecommons.org/licenses/by/4.0/>).

**Keywords:** lithium-ion battery; NMC811; ageing; cold cycling

## 1. Introduction

Given stringent emission standards and de-carbonization policies, there is a major movement towards low-carbon powertrain systems in the transportation and passenger vehicle industries [1]. Hybrid and electric vehicles (EVs) powered by lithium-ion (Li-ion) batteries have already been available on the market for a decade. Despite a relatively low market share, electric powertrain systems are expected to achieve a larger share due to the continuously reduced cost and improved performance [2]. To meet the growing demand for EVs, more original equipment manufacturers are developing next-generation Li-ion and EV technologies.

Li-ion battery chemistries are superior to others due to their favourable characteristics, such as high energy and power density and low self-discharge [3,4]. Cathode materials are amongst the most important constituents affecting Li-ion battery performance. Several Li-ion chemistries are of interest, including but not limited to lithium nickel manganese, cobalt lithium iron phosphate, lithium nickel cobalt aluminium oxide, lithium manganese oxide, lithium titanate, lithium cobalt oxide and lithium-air. Cost, energy and power density, life cycle and environmental impact are considered factors in the development of Li-ion battery chemistry [5]. Among those Li-ion chemistries,  $\text{LiNi}_x\text{Mn}_y\text{Co}_z\text{O}_2$  cathodes have a significant market share [1]. Following the commercial success of  $\text{LiNi}_{1/3}\text{Mn}_{1/3}\text{Co}_{1/3}\text{O}_2$  (NMC111, where  $x = 1/3$ ,  $y = 1/3$ , and  $z = 1/3$ ) chemistry, NMC cathodes have become mainstream chemistries used in cars such as BMW i3, Chevy Bolt, Nissan Leaf, and Tesla Powerwall. To push energy density to a higher level, NMC chemistries with a higher high-nickel content have been researched and developed, for example, NMC433, NMC532, NMC622 and

NMC811. NMC811 composes state of the art NMC chemistry [6–8]. Compared to matured NMC111 chemistry,  $\text{LiNi}_{0.8}\text{Mn}_{0.1}\text{Co}_{0.1}\text{O}_2$  (NMC811, where  $x = 0.8$ ,  $y = 0.1$ , and  $z = 0.1$ ) features a higher specific capacity ( $\approx 200$  mAh/g vs. 145 mAh/g) [9]. Therefore, NMC811 offers a technological solution for improving the EV mileage range without adding extra battery weight. Furthermore, reducing Co in NMC offers an advantageous cost reduction. While Ni and Mn prices are relatively low and steady, the price of Co is highly volatile, increasing from \$35K/t to \$75K/t in 2017 alone.

NMC811 faces the challenge of accelerated capacity degradation resulting from its relatively poorer structural instability [9]. The cobalt in NMC chemistries provides structural stability, and the manganese offers thermal stability. The structural instability is caused by oxygen evolution. Theoretically, reducing the cobalt and manganese content leads to compromised structural and thermal stabilities. This needs to be quantitatively identified for assessing the overall performance of NMC811. At the current stage, NMC811 is still in its infancy of research and development; therefore, limited data is available for its electrochemical performance, especially its degradation characteristics.

Li-ion battery degradation is governed by several interactive physical and chemical mechanisms [10,11]. From the battery operating/usage disposition, many factors lead to battery ageing, including high/low temperature, current load, over-charge/over-discharge and mechanical stress. Some commonly reported battery degradation mechanisms include solid electrolyte interface (SEI) growth and decomposition, electrolyte and binder decomposition, graphite exfoliation, lithium plating, electrode particle cracking and loss of electric contact. These degradation mechanisms explain the root cause of battery capacity and power fade, which are direct consequences of the loss of lithium inventory and active electrode materials.

Among the above factors related to Li-ion battery degradation, the temperature is one of the most significant [10,12]. Li-ion batteries have a narrow favourable working temperature window (15–40 °C). At a high temperature, Li-ion batteries suffer from capacity attenuation and self-discharge [13]. High temperature also increases chemical and structural instability, which accelerate the risk of degradation, cell swelling and, in the worst scenarios, thermal runaway. Low temperature also significantly affects the performance of Li-ion batteries [14,15]. The cycling of Li-ion batteries at a sub-zero temperature is not recommended due to reduced usable capacity, lithium plating and degradation. Li-ion batteries are charged and discharged by the intercalation and de-intercalation of lithium ions on the positive and negative electrodes, respectively. Low temperatures (e.g., <0 °C) lead to reduced electrolyte conductivity [12,16], charge-transfer kinetics and Li-ion diffusion in the carbon anode, resulting in an increase in the internal resistance and a reduction in the equilibrium potential and discharge capacity [14,15,17]. Charging at low temperatures can lead to undesirable anode lithium plating [18–21] and hence a reduced battery lifespan. In addition, operating at low temperatures can also lead to capacity losses. The usable capacity can be decreased by approximately 23% when the operating temperature is decreased from 25 to −15 °C [17]. Furthermore, low temperatures can lead to safety risks. Lithium dendrites could potentially pierce through the separator and cause a short circuit, which can lead to thermal runaway or even fire [10,12].

NMC cycle and service life need to be fully assessed for their feasible application in EVs. Beyond the vehicle warranty, there is an environmental aspect to be considered. Batteries of EVs need to be durable for allowing EVs to reach the life-cycle emissions break-even point compared to gasoline and diesel vehicles. Battery degradation can reduce the overall utility of EVs. However, this does not significantly affect upstream emissions associated with charging the vehicle. Hence, understanding the battery degradation mechanisms and quantifying battery lifetime in real-world conditions is key to evaluating the economic, social and environmental impact of electric mobility.

This study aims to address the research gap regarding data limitations on NMC811 cold cycling degradation. More specifically, we aged commercial cylindrical 21700 NMC811 5Ah cells at 0 °C under 0.5 C and 1 C current rates and detected 49% capacity fade after

only 200 cycles, plus an interesting self-heating correlation. The article is structured as follows. The experimental setup and procedures are introduced in Section 2. Results and discussion are presented in Section 3. Finally, in Section 4 the key findings are summarised.

## 2. Experimental Setup and Procedures

The batteries tested in this study are commercial 21700 NMC811 5Ah cells. To give more information about the performance of cells cycled at room temperature, results obtained from cycling at 25 °C are presented in the Appendix A (Figures A1 and A2). NMC811 shows a 28% reduction in capacity when cycling at 1 C and 25 °C, compared to 7% at 0.5 C and 25 °C.

Nickel tabs (22 mm × 8 mm × 0.15 mm) were welded to the battery electrical terminals using an MTI spot welder. Low resistant brass blocks were bolted at constant torque to clear acrylic sheets with positioning holes. Figure 1. shows the flowchart of experimental procedures, which mainly include snapshot tests and ageing cycling tests, along with logical criteria of continuing or stopping tests.

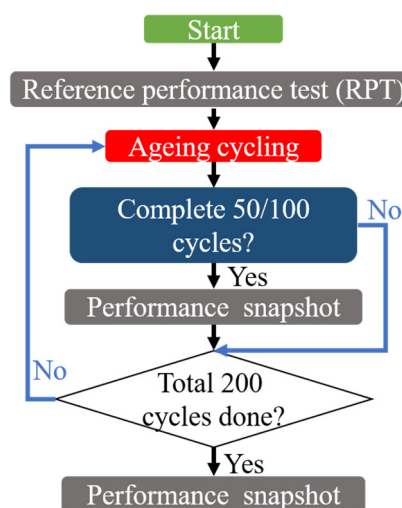


Figure 1. Flowchart of experimental procedures.

**Snapshot test:** Battery capacity, impedance and differential capacity curve are measured in a BioLogic VMP3 with 5 A boosters controlled by an EC-Lab®. Batteries were placed in a Binder thermal chamber (Model MK720) with a set temperature of 25 °C. The test protocol for capacity measurement included a constant-current constant-voltage (CC-CV) charging (current: 1/3 C; upper voltage limit: 4.2 V; cut-off current: 50 mA), a 5 min rest, and a constant-current (CC) discharge (current: 1/3 C; lower voltage limit: 2.5 V). Five repeats were conducted for each battery during snapshot tests. The differential capacity (dQ/dV) curve was determined from the capacity test. The Origin lab Savitzky-Golay filter [11] and EC lab battery analysis package were used to remove noise from the differential capacity curves. Electrochemical impedance spectroscopy (EIS) was used to measure battery impedance. EIS was performed on batteries in frequencies ranging from 10 mHz to 100 kHz (10 points per decade) with a current amplitude of 100 mA (approximately C/50).

**Ageing test:** Battery ageing tests were carried out in 8 channel Neware (BTS4000) cyclers. Cells were placed in a Binder thermal chamber with a predefined temperature. The test protocol for ageing cycling consisted of a CC-CV charging (upper voltage limit: 4.2 V; cut-off current: 1/20 C) and a constant-current (CC) discharge (lower voltage limit: 2.85 V). In the same test, the C rate setting for both charging and discharging was the same. In this study, current rates of 1 C and 0.5 C were tested. Between charge and discharge, there was a 5 min rest.

**Cell Opening:** Batteries were discharged to 0% SOC at the current rate of 1/10 C before being opened to reduce spark/fire risks caused by accidental short-circuit. Cell

opening was conducted in a glovebox under an argon atmosphere, with moisture and oxygen levels below 1 ppm. Electrode jerry rolls were unfolded, after which the anode, cathode and separator were harvested.

**SEM and EDX inspection:** Electrode samples were cut after cell deconstruction inside the glovebox, then transferred to SEM and EDX for analysis. ZEISS FE-Sigma 500 at Coventry University and Zeiss Ultra 55 at Johnson Matthey with a Bruker XFlashI600 Energy Dispersive spectrometer were used. SEM was operated at an accelerating voltage of 15 kV. Secondary electron and backscatter detectors were used for imaging.

### 3. Results

This part consists of three sub-sections. Firstly, battery capacity evolution during ageing tests, snapshot capacity and differential capacity curves (measured at the standard condition) are presented. Secondly, impedance snapshot results are discussed. Thirdly, visual and SEM assessment results are presented.

#### 3.1. Capacity

Cell capacity measured during cold ageing tests is shown in Figure 2. The ageing experiments were paused periodically at an interval of 50/100 cycles for capacity and impedance snapshot measurements. A partial recovery of the cell capacity was observed just after each snapshot test, as is shown clearly in Figure 2b and less obviously in Figure 2a. This cell capacity jump is related to the battery relaxation effect and quickly diminishes after several cycles. The magnitude of such a capacity jump potentially corresponds to factors including, but not limited to, temperature, battery material, pre-relaxation operating condition and relaxation time. Reicher et al. [22] reported that relaxation of more than 2 h was needed for observing a measurable capacity relaxation effect. In this study, the relaxation time was more than 24 h. The relaxation effect is more obvious after a high current charge-discharge test (see Figure 2b), caused by a higher cell polarization.

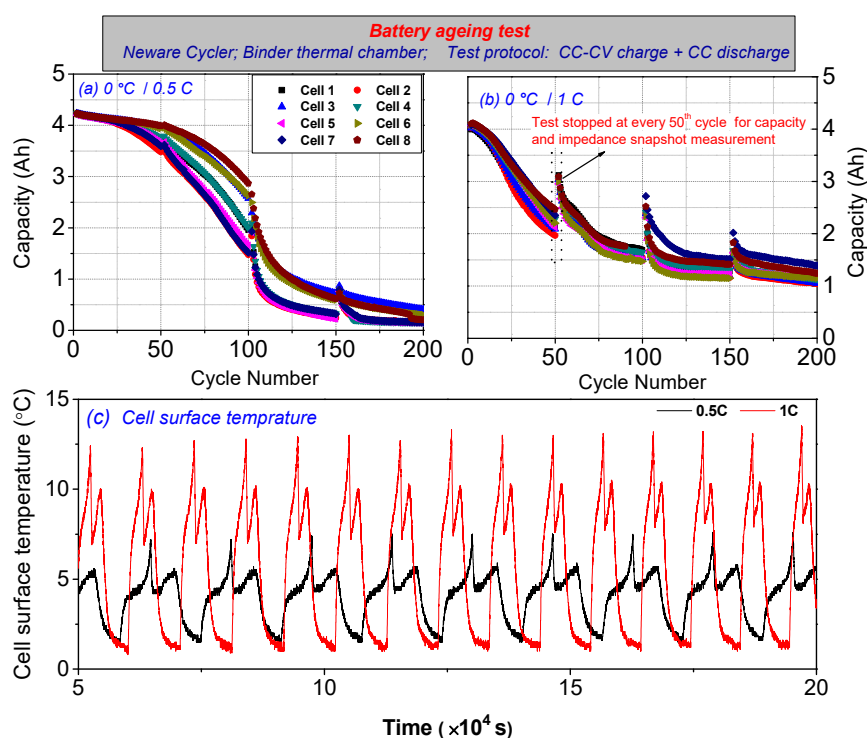


**Figure 2.** Battery status during 0 °C cyclings under a CC-CV charge and CC discharge test protocol. (a) Capacity cycled at 0.5 C; (b) capacity cycled at 1 C; (c) cell surface temperature.

It is reported that the relaxation effect is also related to the diffusion mechanism in the cathode and solid electrolyte interface (SEI) in the anode [22,23]. Active material particles have polycrystalline configurations, where lithium ions can be trapped at inter-crystalline boundaries and blocked diffusion channels. However, the ions can move around the blocked sites via kinetically non-preferential diffusion pathways. This can lead to the temporarily irreversible storage of lithium-ions in the cathode. After a period of relaxation, lithium-ions are again available for cycling by reducing the load carrier-concentration-gradient and kinetic slow diffusion processes. The internal cell impedance is partially affected by the SEI [23]. After a rest, the SEI impedance is possibly lower than during, or shortly after, cycling leading to a higher cell capacity.

It is expected for cells tested at high current rates to experience more severe lithium plating; thus, a larger capacity drop should be observed. However, the opposite phenomenon has been observed in this study. After 200 cycles of tests at 0 °C, the average capacities of cells tested at 0.5 C and 1 C dropped from 4250 mAh to 250 mAh and 1250 mAh, respectively. The most likely reason is that even though the thermal chamber temperature was the same at 0 °C for both 0.5 C and 1 C cycling tests, the self-heating in the resulting battery temperature differs. Cells undergoing 1 C ageing tests had an approximately 10 °C higher surface temperature than that undergoing 0.5 C ageing tests, which was shown in Figure 2c. Waldmann et al. investigated the temperature-dependent ageing mechanisms in 18,650 cylindrical NMC111 cells [13]. Cells were aged in the temperature range of −20 °C to 70 °C. They found that below 25 °C, the ageing rates increase with decreasing temperature, while above 25 °C, the ageing is accelerated with increasing temperature. This finding from Waldmann et al. matches well with that from this study that a higher cell temperature cycled in 0 °C leads to slower battery degradation. A subsequent study with internal thermally instrumented cells is planned to further investigate this phenomenon.

Apart from the capacity drop, the trajectory of the capacity change also differs. The capacity of 0.5 C cycled cells show a distinct knee-point, likely caused by a domino-effect ageing mechanism, while the 1 C cycled cell capacity plateaus after an initial drop. In general, the capacity of an individual cell follows a similar trend in both the 0.5 C and 1 C cases; however, cell-to-cell variations are observed. For example, in Figure 2a, at the end of the 50th cycle, the difference in capacity between the cells is up to 500 mAh, which then increases to 1100 mAh at the end of the 100th cycle. However, the gap decreases again to 480 mAh at the end of the 200th cycle. The cell-to-cell variation is less significant for 1 C cycled cells. This shows that, when exposed to harsher temperature conditions (which the 0.5 C cycled cells effectively experienced), the cell degradation rate varies more.

Results for battery capacity snapshot tests taken at the standard conditions, as specified in the battery specification sheet (1/3 C and 25 °C), are shown in Figure 3. For cells that experienced 1 C cold cycling tests (Figure 3b), the first 50 cold cyclings lead to a 10% reduction in capacity; however, a further 50 cycles lead to no statistically significant difference in capacity in all cells except for Cell 1. The reason for the different behaviour of Cell 1 is likely related to the cell manufacturing variation. State-of-health (SOH)—a parameter that quantitatively describes the ‘age’ of a battery, is defined as the discharge capacity of an aged cell in comparison with that of a new cell. A SOH < 80% is commonly regarded as the end-of-life (EOL) criterion for a battery [24]. The standard EOL state (80% remaining capacity) was reached after 200 cycles for cells cycled at 0 °C and 1 C, and after less than 100 cycles for cells cycled at 0 °C and 0.5 C.



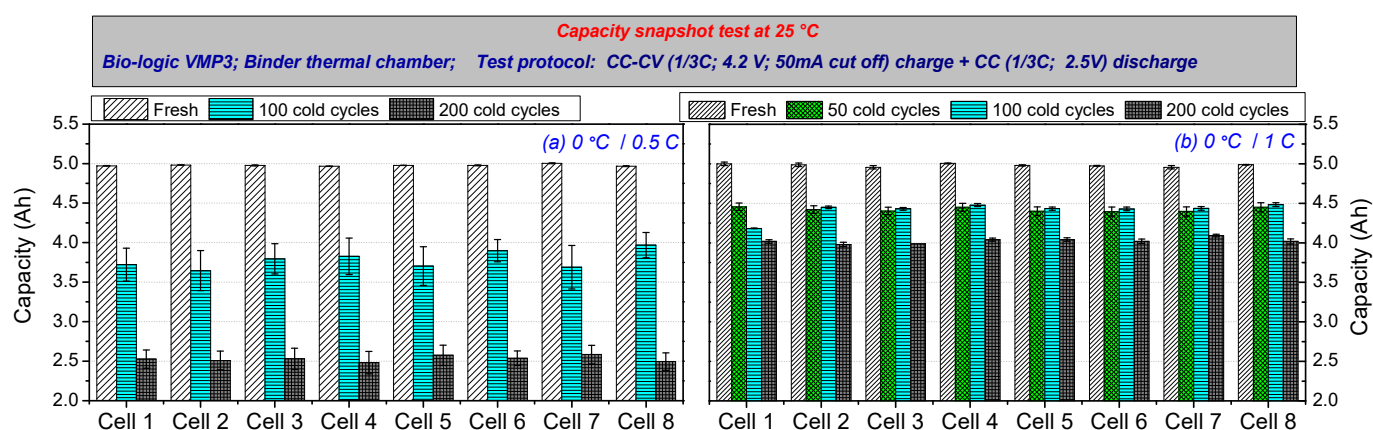


**Figure 3.** Capacity snapshot tested at 25 °C and 1/3 C for batteries that experienced a 0 °C cold cycling under the current rates (a) 0.5 C; (b) 1 C.

For comparison, literature data was taken to assess the cycle life of NMC 811 cells used in this study. The EOL for Panasonic UR18650E NMC111 lithium-ion batteries at the condition of 1 C and 20 °C is 500 cycles according to the specification sheet [25]. Baumhöfer et al. tested the same cells at the condition of 1 C and 25 °C, and they found that the EOL is between 900 and 1300 cycles, subjecting to cell-to-cell variation [26]. Popp et al. [27] reported that the NCM111 battery maintains 80% of its initial capacity after 455 cycles tested with a LIBERAL like PHEV cycle. Popp et al. [27] also found that while the NCM111 battery maintained ~75% of its initial capacity after 700 cycles, a lithium iron phosphate battery reaches ~20% of its initial capacity after 700 cycles. Leng et al. [28] reported that NMC311 reaches 20% of its initial capacity after ~1000 cycles at the condition of 25 °C and 1 C charge/discharge. Even though the test conditions used in the above literature, including charge and discharge condition and temperature are not the same, the cycle life of NMC811 reported in this paper is not satisfactory.

The reduction in capacity shown in Figure 3 is linked to the impacts of low temperature on electrolyte and active anode material. Lithium plating on the anode (due to low temperature) leads to loss of lithium inventory and may lead to dendrite formation, and internal short-circuits, which in turn cause catastrophic cell failure. Loss of lithium inventory results in less lithium being available for cycling between the positive and negative electrodes, leading to irreversible capacity fade. Electrolyte, a medium allowing Li-ion to transport back and forth between the cathode and anode electrodes, has a low ion-conductivity when the temperature is low. Therefore, during charging, the voltage upper limit would be hit earlier due to the low electrolyte ion conductivity. The capacity drop due to low ion-conductivity at low temperature is reversible once the temperature is increased back to ambient.

Furthermore, since the electrolyte contains a mixture of various carbonates, some of the higher freezing point carbonates will be crystallized. As active material in both electrodes is porous, crystallized electrolytes may deposit on the porous active material, leading to loss of active material for Li<sup>+</sup> insertion and extraction. Furthermore, lithium already inserted in that active material is trapped inside and becomes inactive. This kind of reduced capacity is reversible when the battery is returned to normal temperature. Electrolyte crystallization with volume expansion can also happen inside porous electrolytes, leading to cracking in the porous structure. This may lead to active material no longer being available for the insertion of lithium due to particle cracking and loss of electrical contact. The crack-related capacity drop is irreversible.

For each capacity snapshot, five repeats were conducted. Error bars were calculated from the standard deviation of results from five repeats. Figure 3a clearly showed a much larger error than those in Figure 3b. Indeed, a noticeable drop of capacity in five repeats for cells that experienced 0.5 C cold cycling is surprising, considering that the capacity snapshot is done under a mild condition (1/3 C and 25 °C). It is hypothesized that the cells

suffer from permanent internal damage to the electrodes. To further confirm this, at the end of the 200 cycles of 0.5 C cold ageing, the cells were tested at 1/3 C and 25 °C (same as capacity snapshot tests) for 25 cycles, the results of which are presented in Figure 4. The battery capacity shows a significant continuous drop, present in all cells with some level of variation. After 25 cycles at 1/3 C and 25 °C, batteries were stored for three months. At the end of the three-month storage, the cell terminal voltage dropped to 0 V. Klein et al. [29] studied the degradation mechanism of NCM523, and in aged cells, they observed remarkable fluctuations of the charge capacity as well as the cell voltage and current noise. They mentioned that severe dendrite formation and penetration through the SPE is most likely the main source for “voltage noise” and sudden cell failure. They called this failure mode a lithium dendrite micro short circuit. The micro short circuit, in the worst case, even causes a rollover failure. It is hypothesized that a micro short circuit due to cell lithium dendrites might result in the accelerated battery degradation presented in Figure 4. Further studies are needed to examine this assumption.

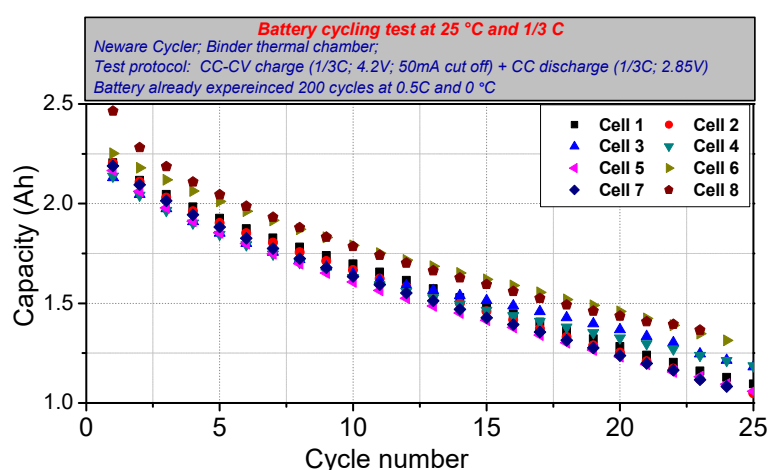


**Figure 4.** Capacity for batteries cycled at 25 °C and 1/3 C (before this test, batteries were cycled 200 times at 0.5 C and 0 °C).

Snapshots of differential capacity curves tested at 25 °C and 1/3 C are presented in Figure 5. There was a noticeable difference in differential capacity curves observed between the fresh cell and the cell that experienced 200 cold cycles. The peak area under the differential curve drops as the cell is cold aged, especially for cells aged at 0.5 C [30]. The peak position in the differential capacity curves shift. For example, during the cell charging, there were four peaks for fresh cells aged at 0.5 C; however, only two peaks were observed after 200 cold cycles, and the existing peaks shifted towards higher voltages.

### 3.2. Impedance

The primary effect of degradation on the cell’s kinetics is an increase in internal resistance or cell impedance. An increase in resistance can also lead to a decrease in useful energy capacities since the lower voltage cut-off of the cell is reached sooner in a cell with higher internal resistance. Equivalently, the higher voltage cut-off is reached sooner during charging. Figure 6a,b shows Nyquist plots of batteries EIS (SOC = 50%) cycled at 0.5 C and 1 C, respectively. Results of other SOCs are shown in the Appendix A (Figure A3).



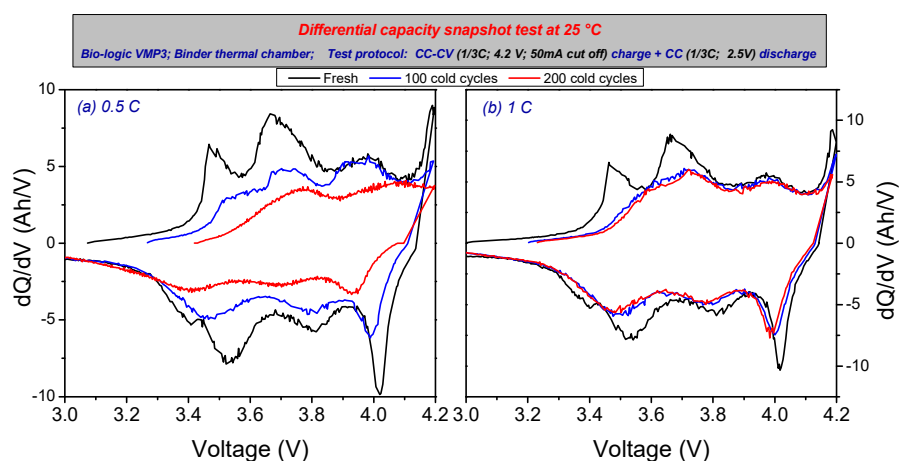


**Figure 5.** Snapshot results of differential capacity curves tested at 25 °C and 1/3 C for batteries experiencing 0 °C cold cyclings under the current rates of (a) 0.5 C and (b) 1 C.

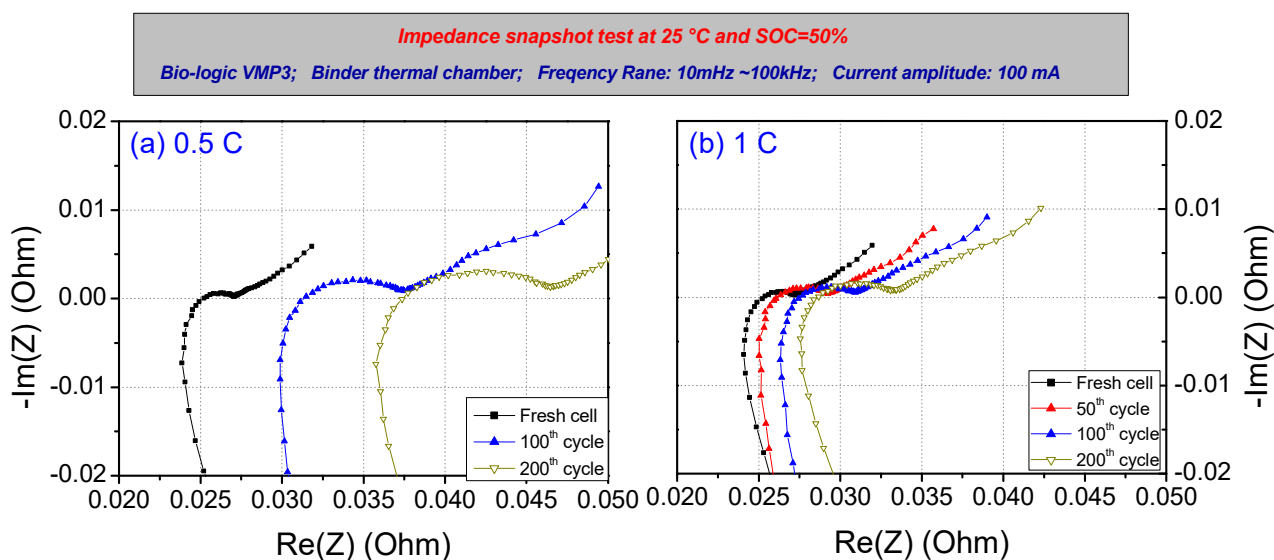


**Figure 6.** Impedance snapshot (SOC = 50%) tested at 25 °C and 1/3 C for batteries experiencing 0 °C cold ageing cycling at (a) 0.5 C and (b) 1 C.

It was observed that, compared to fresh cells, cells that experienced cold cycling have higher impedance, especially when cycled at 0.5 C, which is in line with the capacity drop observations made earlier. As the anodes experience lithium plating, the electrolyte reacts with the dendrites and decomposes. This leads to electrolyte loss and a thicker, more resistive SEI layer. Right shift and expansion of the semi-circle were also observed, which is related to the impedance of charge transfer. Particle cracking, pore-clogging and particle disconnection may lead to an increase in charge transfer [31].  $R_{ohm}$ , the sum of the ohmic resistance of binder, current collector, electrodes and electrolytes can be obtained by solving the intersections between the impedance spectrum and the real axis in the high-frequency region of the Nyquist plot. For example, after 200 cycles at 0 °C,  $R_{ohm}$  increased from 25.1 mΩ to 37.4 and 28.6 mΩ at 200 cycles for cells cycled at 0.5 and 1 C, respectively.

### 3.3. Electrodes Post-Mortem Inspection

Electrode images from new and cold aged cells are shown in Figure 7. There is no visual difference observed in the cathodes for either new or aged cells. However, lithium plating on anodes (white stain) was observed for cold aged cells, which are signs of lithium

plating resulting from cold cycling. Waldmann et al. investigated NMC111 pouch cells with reference electrodes, and they observed that in the anode, there is a negative polarization with respect to  $\text{Li}/\text{Li}^+$  at the temperature range of  $-10$  to  $20\text{ }^{\circ}\text{C}$  [13]. However, at a temperature higher than  $25\text{ }^{\circ}\text{C}$ , there is a positive polarization in the anode with respect to  $\text{Li}/\text{Li}^+$ . They also opened cells and found that the anodes were plated with grey metallic Li. Lin et al. also reported the negative anode potential during charging at  $-20\text{ }^{\circ}\text{C}$  [32].

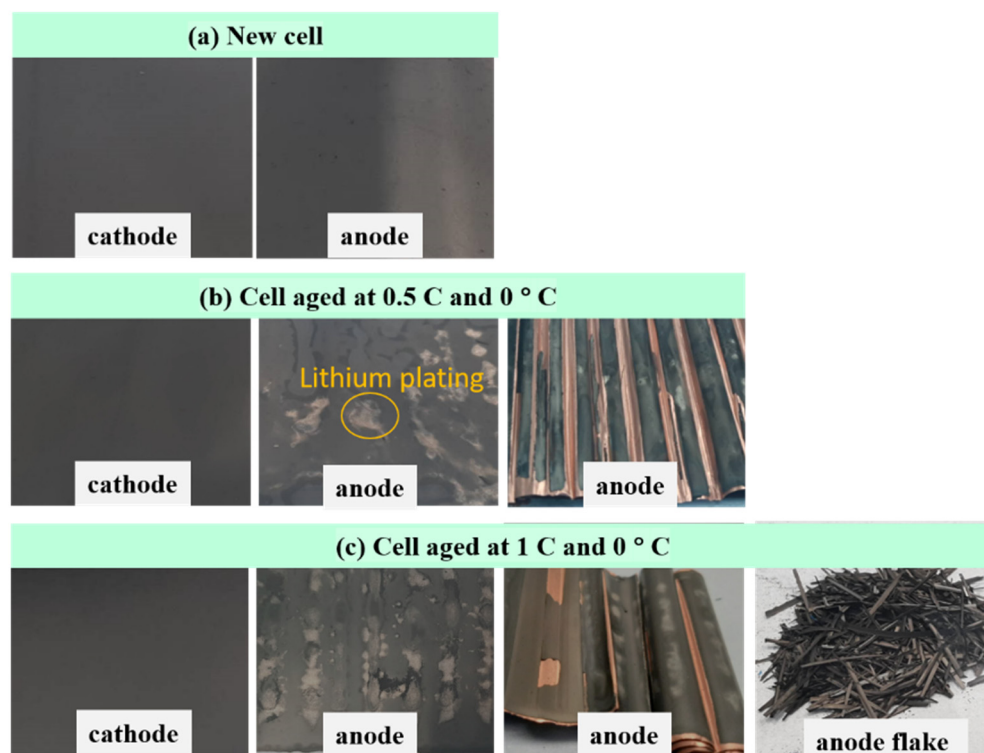


**Figure 7.** Electrodes harvested from new and cold aged cells.

Unlike the new anode, the cold aged anode became rigid and fragile after 200 cold cycles, with the material flaking easily, especially for cells cycled at  $0.5\text{ C}$ . This leads to contact loss between the current collector and active material in the anode, resulting in loss of active material. The centre of the jelly roll is most affected, likely due to the smaller radius resulting in a higher degree of curvature and the associated material stresses.

Figure 8 shows SEM images taken from new and cold aged cells. There is not much change in cold aged cathodes compared to the new ones, except for some cracked particles in the  $0.5\text{ C}$  cycled cell at  $0\text{ }^{\circ}\text{C}$  (Figure 8c). The new anode (Figure 8b) shows the continuous structure, whereas both  $0.5\text{ C}$  and  $1\text{ C}$  cold cycled anodes show distinct cracks. More SEM and EDX spectroscopy results are available in the Appendix A (Figures A4–A6). It should be noted that the images shown in Figure 8 were taken by a ZEISS FE-Sigma 500 at Coventry University, and those in Figures A4–A6 were taken by a ZEISS Ultra 55 at Coventry University.

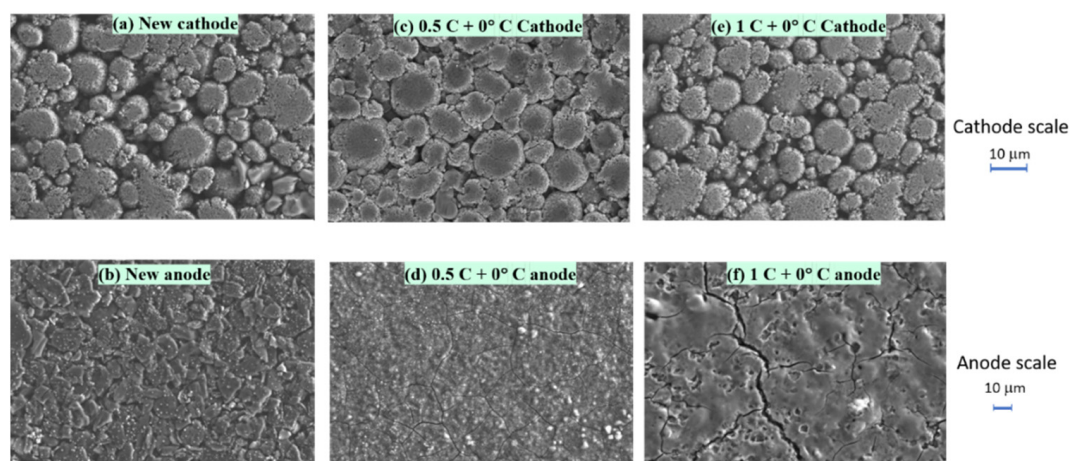


**Figure 8.** SEM images for electrodes from new and cold aged cells (ZEISS FE-Sigma 500; acceleration voltage of secondary electron detector: 15 kV).

#### 4. Conclusions

In this paper, a cold ageing study was conducted on commercial 21700 cylindrical NMC811 5Ah Li-ion batteries at two current rates (0.5 C and 1 C). Electrode post-mortem visual and SEM inspections were carried out. The following are the main conclusions.

1. After just 200 cycles at 0 °C, the NMC811 battery capacity was reduced by 20% (1 C) and 49% (0.5 C). The standard end-of-life state of 80% remaining capacity was reached after less than 100 cycles for cells cycled at 0 °C and 0.5 C. The reason behind the more significant capacity loss during 0.5 C cycling is due to the reduced cell self-heating.
2. Cell impedance increases during cold cycling, especially for cells cycled at 0.5 C. After 200 cyclings at 0 °C, the ohmic resistance increased from 25.1 to 37.4 mΩ and 28.6 mΩ for cells cycled at 0.5 and 1 C, respectively. Increased impedance further limits accessible cell capacity.
3. The differential capacity peak curves fall significantly, and the peak position shift as the cell ages, which reflects the damage to the active material and its structure.
4. Cells that experienced cold ageing showed a noticeable negative impact on the anode, where active material became rigid and readily delaminated. Active material delamination is more obverse at the inner part of the jerry roll. SEM inspection confirmed significant anode cracking, leading to active materials and lithium inventory loss, and an increase in the negative electrode resistance. Lithium plating was also observed on the anode. Only minor cracks in cathode particles were observed.

**Author Contributions:** Conceptualization, C.W.; data curation, R.C. and G.G.; formal analysis, C.W., T.A., R.C. and C.Z.; funding acquisition, R.B.; methodology, T.A., R.C., Y.G., Z.A. and G.G.; resources, Y.G. and R.B.; writing—original draft, C.W.; writing—review & editing, T.A., R.C., Y.G., Z.A., C.Z. and R.B. All authors have read and agreed to the published version of the manuscript.

**Funding:** This research was funded by the Innovate UK (<https://gtr.ukri.org/projects?ref=104176> (accessed on 1 August 2021) under the project ‘CALIBRE—Custom Automotive Lithium-Ion Battery Recycling (Grant Reference Number: 104176)’, and the EPSRC project TRENDS (Grant Reference Number: EP/R020973/1).

**Institutional Review Board Statement:** Not applicable.

**Informed Consent Statement:** Not applicable.

**Data Availability Statement:** Data sharing not applicable.

**Conflicts of Interest:** The authors declare no conflict of interest. The funders had no role in the design of the study; in the collection, analyses, or interpretation of data; in the writing of the manuscript, or in the decision to publish the results.

## Appendix A

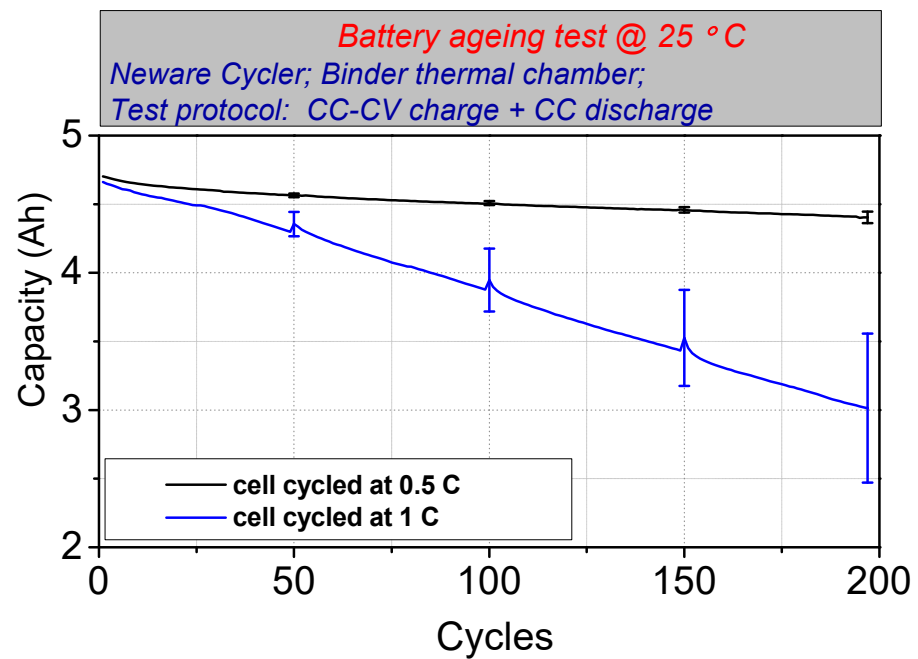


Figure A1. Battery capacity in the 25 °C cycling ageing test.

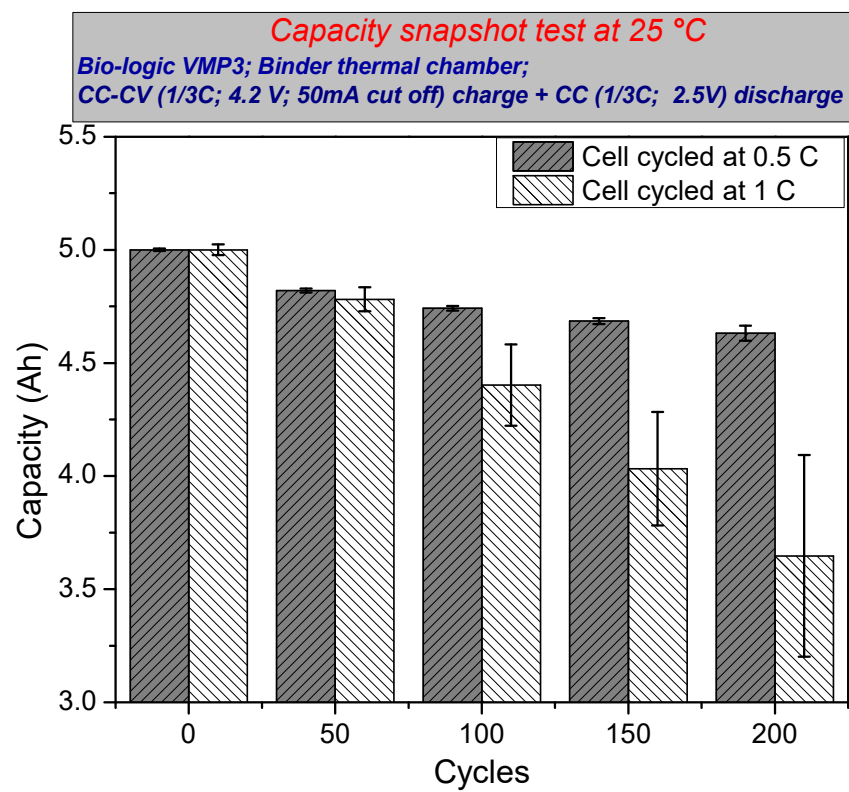
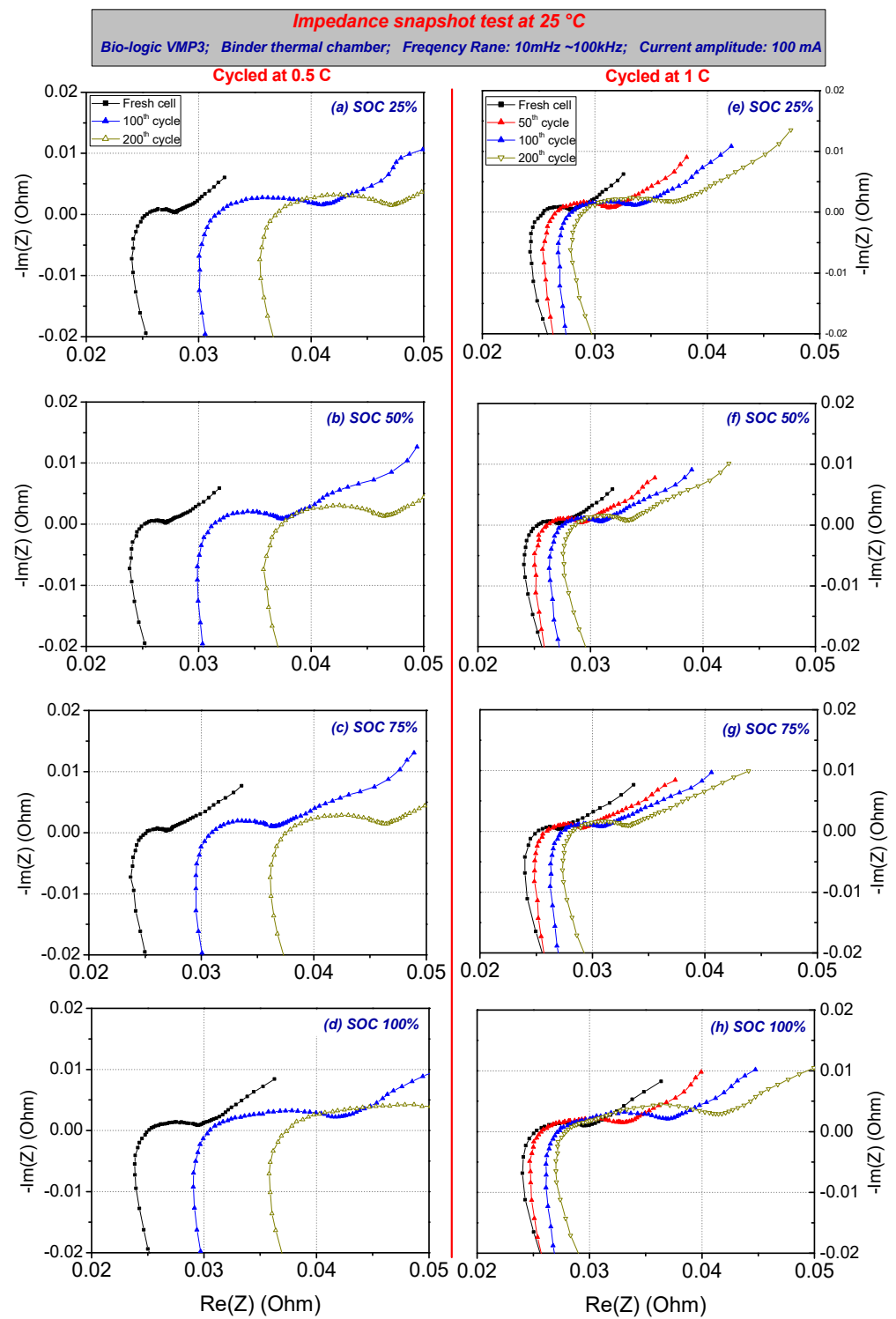
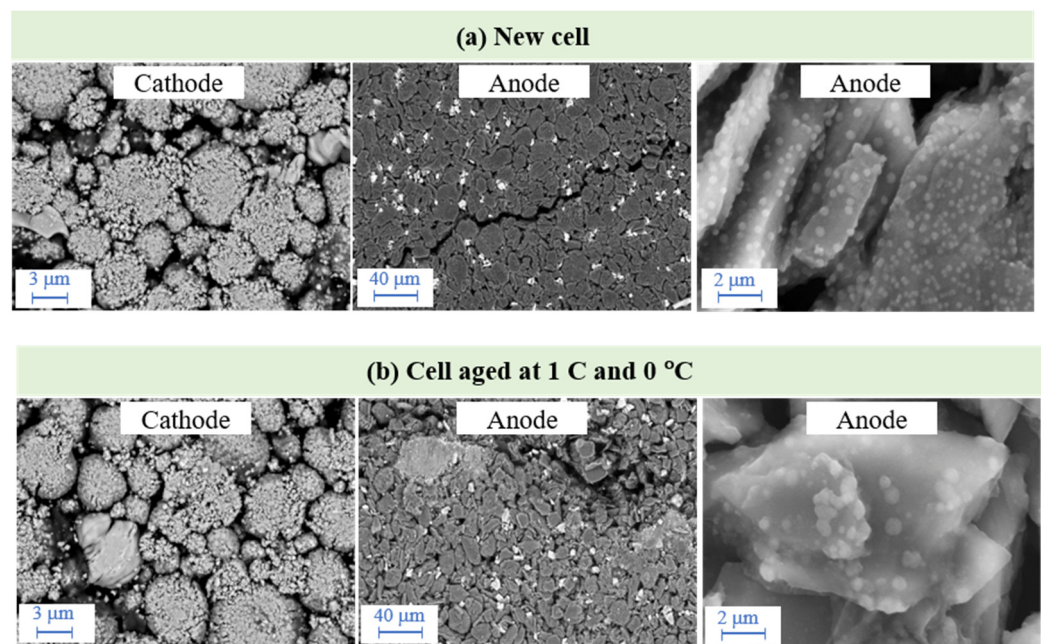


Figure A2. Capacity snapshot tested at 25 °C and 1/3 C for batteries that experienced 25 °C cyclings under the current rates of 0.5 C and 1 C.



**Figure A3.** Impedance snapshot at various SOC levels for batteries experienced 0 °C cold ageing.





**Figure A4.** SEM images for electrodes from new and cold aged cells (SEM: ZEISS Ultra 55; acceleration voltage of secondary electron detector: 15 kV).

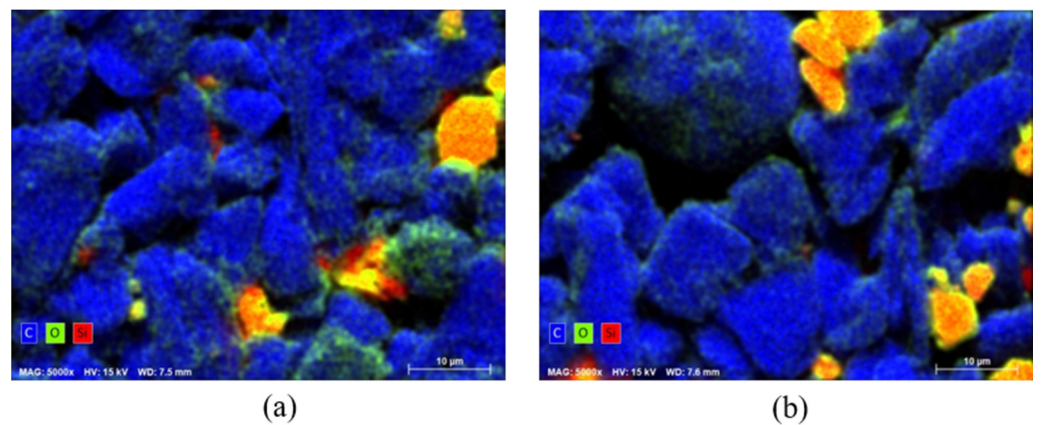


**Figure A5.** EDX mapping at 5000 $\times$  magnification. (a) New anode; (b) cold aged anode cycled at 1 C and 0 °C.



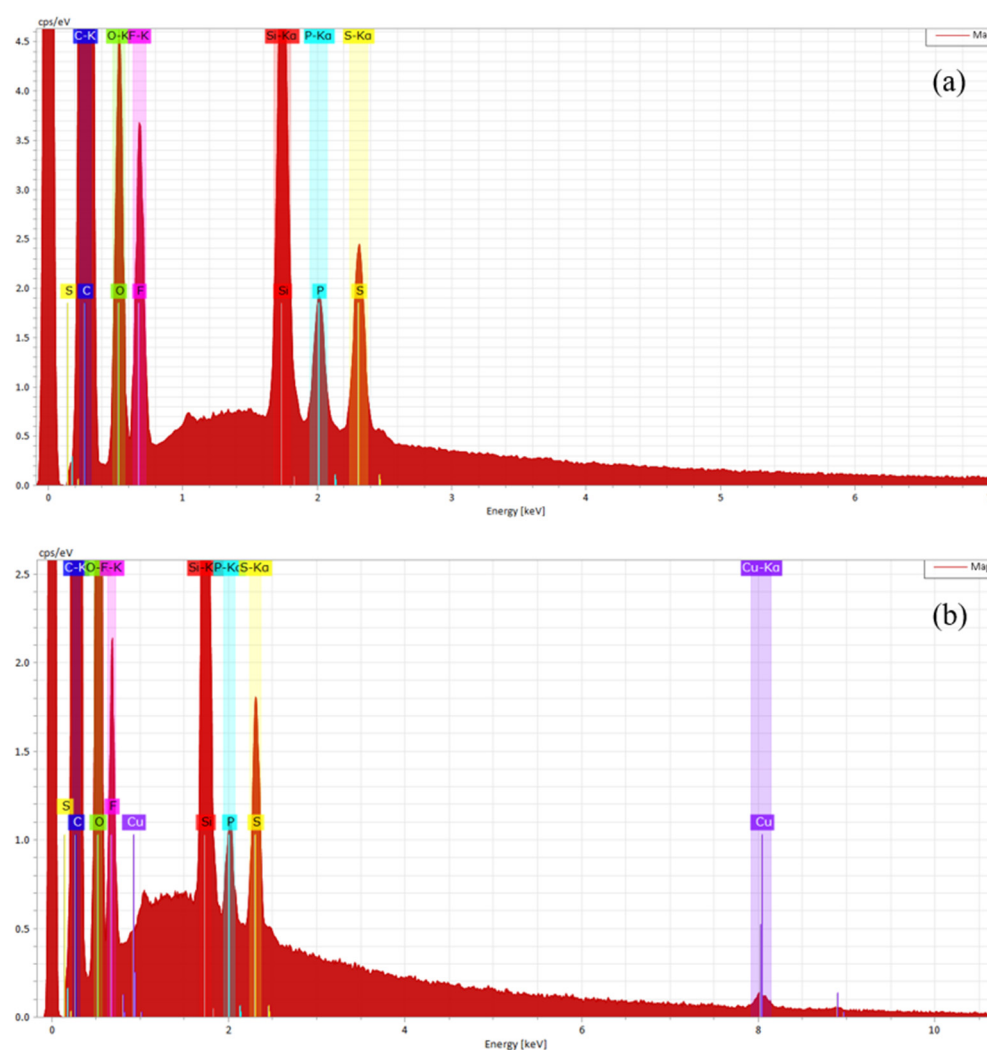


Figure A6. EDX spectroscopy of cells. (a) New anode; (b) cold aged anode cycled at 1 C and 0 °C.

## References

1. IEA, Global EV Outlook 2020. Available online: <https://www.iea.org/reports/global-ev-outlook-2020> (accessed on 21 June 2021).
2. Duffner, F.; Wentker, M.; Greenwood, M.; Leker, J. Battery cost modeling: A review and directions for future research. *Renew. Sustain. Energy Rev.* **2020**, *127*, 109872. [CrossRef]
3. Fleming, J.; Amietszajew, T.; Charmet, J.; Roberts, A.J.; Greenwood, D.; Bhagat, R. The design and impact of in-situ and operando thermal sensing for smart energy storage. *J. Energy Storage* **2019**, *22*, 36–43. [CrossRef]
4. Opitz, A.; Badami, P.; Shen, L.; Vignarooban, K.; Kannan, A.M. Can Li-Ion batteries be the panacea for automotive applications? *Renew. Sustain. Energy Rev.* **2017**, *68*, 685–692. [CrossRef]
5. Budde-Meiwes, H.; Drillkens, J.; Lunz, B.; Muennix, J.; Rothgang, S.; Kowal, J.; Sauer, D.U. A review of current automotive battery technology and future prospects. *Proc. Inst. Mech. Eng. Part D J. Automob. Eng.* **2013**, *227*, 761–776. [CrossRef]
6. Yuan, A.; Tang, H.; Liu, L.; Ying, J.; Tan, L.; Tan, L.; Sun, R. High performance of phosphorus and fluorine co-doped  $\text{LiNi}_{0.8}\text{Co}_{0.1}\text{Mn}_{0.1}\text{O}_2$  as a cathode material for lithium ion batteries. *J. Alloys Compd.* **2020**, *844*, 156210. [CrossRef]
7. Zhao, S.; Zhu, Y.; Qian, Y.; Wang, N.; Zhao, M.; Yao, J.; Xu, Y. Annealing effects of  $\text{TiO}_2$  coating on cycling performance of Ni-rich cathode material  $\text{LiNi}_{0.8}\text{Co}_{0.1}\text{Mn}_{0.1}\text{O}_2$  for lithium-ion battery. *Mater. Lett.* **2020**, *265*, 127418. [CrossRef]
8. Nanthagopal, M.; Santhoshkumar, P.; Shaji, N.; Sim, G.S.; Park, J.W.; Senthil, C.; Lee, C.W. An encapsulation of nitrogen and sulphur dual-doped carbon over  $\text{Li}[\text{Ni}_{0.8}\text{Co}_{0.1}\text{Mn}_{0.1}]\text{O}_2$  for lithium-ion battery applications. *Appl. Surf. Sci.* **2020**, *511*, 145580. [CrossRef]
9. Sun, H.; Wang, J.; Liu, Q.; Zhang, Y.; Zhang, D.; Wang, Q.; Li, Z.; Li, W.; Wang, B. Ag–Sn dual-modified  $\text{LiNi}_{0.8}\text{Co}_{0.1}\text{Mn}_{0.1}\text{O}_2$  as cathode for lithium storage. *J. Alloys Compd.* **2021**, *850*, 156763. [CrossRef]
10. Birkel, C.R.; Roberts, M.R.; McTurk, E.; Bruce, P.G.; Howey, D.A. Degradation diagnostics for lithium ion cells. *J. Power Source* **2017**, *341*, 373–386. [CrossRef]
11. Xiong, R.; Pan, Y.; Shen, W.; Li, H.; Sun, F. Lithium-ion battery aging mechanisms and diagnosis method for automotive applications: Recent advances and perspectives. *Renew. Sustain. Energy Rev.* **2020**, *131*, 110048. [CrossRef]

12. Petzl, M.; Kasper, M.; Danzer, M.A. Lithium plating in a commercial lithium-ion battery—A low-temperature aging study. *J. Power Source* **2015**, *275*, 799–807. [\[CrossRef\]](#)
13. Waldmann, T.; Wilka, M.; Kasper, M.; Fleischhammer, M.; Wohlfahrt-Mehrens, M. Temperature dependent ageing mechanisms in Lithium-ion batteries—A Post-Mortem study. *J. Power Source* **2014**, *262*, 129–135. [\[CrossRef\]](#)
14. Burow, D.; Sergeeva, K.; Calles, S.; Schorb, K.; Börger, A.; Roth, C.; Heitjans, P. Inhomogeneous degradation of graphite anodes in automotive lithium ion batteries under low-temperature pulse cycling conditions. *J. Power Source* **2016**, *307*, 806–814. [\[CrossRef\]](#)
15. Ouyang, M.; Chu, Z.; Lu, L.; Li, J.; Han, X.; Feng, X.; Liu, G. Low temperature aging mechanism identification and lithium deposition in a large format lithium iron phosphate battery for different charge profiles. *J. Power Source* **2015**, *286*, 309–320. [\[CrossRef\]](#)
16. Zhang, S.S.; Xu, K.; Jow, T.R. Electrochemical impedance study on the low temperature of Li-ion batteries. *Electrochim. Acta.* **2004**, *49*, 1057–1061. [\[CrossRef\]](#)
17. Ma, S.; Jiang, M.; Tao, P.; Song, C.; Wu, J.; Wang, J.; Deng, T.; Shang, W. Temperature effect and thermal impact in lithium-ion batteries: A review. *Prog. Nat. Sci. Mater. Int.* **2018**, *28*, 653–666. [\[CrossRef\]](#)
18. Jones, P.; Smart, M.C.; Krause, F.C.; Bugga, R.V. The Effect of Electrolyte Additives upon Lithium Plating during Low Temperature Charging of Graphite-LiNiCoAlO<sub>2</sub> Lithium-Ion Three Electrode Cells. *J. Electrochem. Soc.* **2020**, *167*, 020536. [\[CrossRef\]](#)
19. Koleti, U.R.; Rajan, A.; Tan, C.; Moharana, S.; Dinh, T.Q.; Marco, J. A Study on the Influence of Lithium Plating on Battery Degradation. *Energies* **2020**, *13*, 3458. [\[CrossRef\]](#)
20. Koleti, U.R.; Zhang, C.; Malik, R.; Dinh, T.Q.; Marco, J. The development of optimal charging strategies for lithium-ion batteries to prevent the onset of lithium plating at low ambient temperatures. *J. Energy Storage* **2019**, *24*, 100798. [\[CrossRef\]](#)
21. Downie, L.E.; Krause, L.J.; Burns, J.C.; Jensen, L.D.; Chevrier, V.L.; Dahn, J.R. In Situ Detection of Lithium Plating on Graphite Electrodes by Electrochemical Calorimetry. *J. Electrochem. Soc.* **2013**, *160*, A588–A594. [\[CrossRef\]](#)
22. Reichert, M.; Andre, D.; Rösmann, A.; Janssen, P.; Bremes, H.G.; Sauer, D.U.; Passerini, S.; Winter, M. Influence of relaxation time on the lifetime of commercial lithium-ion cells. *J. Power Source* **2013**, *239*, 45–53. [\[CrossRef\]](#)
23. Vetter, J.; Novák, P.; Wagner, M.R.; Veit, C.; Möller, K.C.; Besenhard, J.O.; Winter, M.; Wohlfahrt-Mehrens, M.; Vogler, C.; Hammouche, A. Ageing mechanisms in lithium-ion batteries. *J. Power Source* **2005**, *147*, 269–281. [\[CrossRef\]](#)
24. Duong, T.Q. USABC and PNGV test procedures. *J. Power Source* **2000**, *89*, 244–248. [\[CrossRef\]](#)
25. Panasonic, Lithium-Ion Battery UR18650E Data Sheet. 2014. Available online: [https://voltaplex.com/media/whitepapers/specification-sheet/Sanyo\\_E\\_Specification\\_Sheet.pdf](https://voltaplex.com/media/whitepapers/specification-sheet/Sanyo_E_Specification_Sheet.pdf) (accessed on 5 May 2021).
26. Baumhöfer, T.; Brühl, M.; Rothgang, S.; Sauer, D.U. Production caused variation in capacity aging trend and correlation to initial cell performance. *J. Power Source* **2014**, *247*, 332–338. [\[CrossRef\]](#)
27. Popp, H.; Attia, J. Lifetime analysis of four different lithium ion batteries for plug-in electric vehicle. In Proceedings of the Transport Research Arena (TRA) 5th Conference: Transport Solutions from Research to Deployment, Paris, France, 14–17 April 2014.
28. Leng, Y.; Ge, S.; Marple, D.; Yang, X.-G.; Bauer, C.; Lamp, P.; Wang, C.-Y. Electrochemical Cycle-Life Characterization of High Energy Lithium-Ion Cells with Thick Li(Ni<sub>0.6</sub>Mn<sub>0.2</sub>Co<sub>0.2</sub>)O<sub>2</sub> and Graphite Electrodes. *J. Electrochem. Soc.* **2017**, *164*, A1037–A1049. [\[CrossRef\]](#)
29. Klein, S.; Bärman, P.; Beuse, T.; Borzutzki, K.; Frerichs, J.E.; Kasnatscheew, J.; Winter, M.; Placke, T. Exploiting the Degradation Mechanism of NCM523Graphite Lithium-Ion Full Cells Operated at High Voltage. *ChemSusChem* **2021**, *14*, 595–613. [\[CrossRef\]](#)
30. Li, J.; Harlow, J.; Stakheiko, N.; Zhang, N.; Paulsen, J.; Dahn, J. Dependence of Cell Failure on Cut-Off Voltage Ranges and Observation of Kinetic Hindrance in LiNi<sub>0.8</sub>Co<sub>0.15</sub>Al<sub>0.05</sub>O<sub>2</sub>. *J. Electrochem. Soc.* **2018**, *165*, A2682–A2695. [\[CrossRef\]](#)
31. Liu, J.; Duan, Q.; Chen, H.; Sun, J.; Wang, Q. An optimal multistage charge strategy for commercial lithium ion batteries. *Sustain. Energy Fuels* **2018**, *2*, 1726–1736. [\[CrossRef\]](#)
32. Lin, H.-P.; Chua, D.; Salomon, M.; Shiao, H.-C.; Hendrickson, M.; Plichta, E.; Slane, S. Low-temperature behavior of Li-ion cells. *Electrochem. Solid-State Lett.* **2001**, *4*, A71–A73. [\[CrossRef\]](#)